The Properties of Electrodeposited Zn-Co Coatings

J. Mahieu, K. De Wit, A. De Boeck, and B.C. De Cooman

(Submitted 26 January 1999; in revised form 10 May 1999)

The possibility of increasing the corrosion resistance of automotive sheet steel by electrodepositing with Zn-Co alloy coatings was investigated. Process variables during electrodeposition such as current density, electrolyte flow rate, and pH were varied in order to examine their influence on the electroplating process. Cobalt contents varying from 0.2 to 7 wt% were easily obtained. The influence of these process parameters on the characteristics of the coating could be related to the hydroxide suppression mechanism for anomalous codeposition. The structure and the morphology of the coatings were determined using SEM and XRD analysis. Application properties important for coating systems used in the automotive industry, such as friction behavior, adhesion, and corrosion behavior, were investigated on coatings with varying cobalt content. The corrosion resistance of the Zn-Co alloy layers was found to be better than that of pure zinc coatings.

Keywords corrosion resistance, electrodeposited coatings, Zn-Al coatings, Zn-Co coatings

1. Introduction

Zinc and zinc alloy coatings are increasingly being used in the automotive industry to protect the car body from both perforation corrosion and cosmetic corrosion. In recent years there has been a growing interest in replacing pure zinc coatings with thinner, more corrosion-resistant zinc-alloy layers (Ref 1-3). Zinc-iron alloy layers, both electroplated and galvannealed, and electroplated zinc-nickel coatings are currently widely used in the automotive industry (Ref 4, 5).

Zinc-cobalt alloys, however, are by far the most widely used zinc alloys for plating in North America to meet the increased demands for corrosion resistance (Ref 6). However, these layers are not currently used to plate sheet steel, but there is a widespread use of zinc-cobalt alloy coatings for nuts and bolts.

As a consequence, a review of literature on this subject shows that little information is available on the use of zinc-cobalt alloy coatings on sheet steel. Moreover, the information is limited to a small range of cobalt in the coating, varying from 0 to 2 wt% (Ref 3, 7-9).

This article focuses on the influence of cobalt content on the application properties of zinc-cobalt alloy electroplated sheet steel and evaluates the potential of zinc-cobalt electroplatings as coatings for automotive applications.

First, the influence of process parameters such as bath composition, pH, current density, and flow rate of the electrolyte on the morphology and the cobalt content of the coatings is examined. Second, this study evaluates the influence of coating composition on the roughness, friction, powdering, and galling behavior as well as on the shear strength. The corrosion rate of the deposits was examined by electrochemical measurements.

J. Mahieu, K. De Wit, and **B.C. De Cooman,** Laboratory for Iron and Steel Making, University of Ghent, Ghent, Belgium; and **A. De Boeck,** OCAS N.V. (Sidmar Group), Zelzate, Belgium. Contact e-mail: bcdc@ocas.be.

2. Experimental Procedure

2.1 Electroplating Equipment

The zinc-cobalt alloy coatings were produced on a laboratory electroplating line at the University of Ghent in Belgium. The vertical flow cell was designed for one-side electroplating. The plated area was 50 by 150 mm^2. High flow rates and high current densities were obtainable. The required current was achieved by use of a Siemens Simoreg K rectifier. The anode was made of stainless steel and the anode-to-cathode spacing was 15 mm. Electroplating was carried out on previously degreased and acid-pickled sheet steel substrate.

All electroplating experiments were done using a sulfate bath containing 125 g/L $CoSO_4 \cdot 7H_2O$ and 625 g/L $ZnSO_4 \cdot 7H_2O$. Sodium sulfate (75 g/L) was added to improve the conductivity.

Since the plating conditions could influence the composition and quality of the deposits, pH, flow rate, and current density were varied in order to obtain a wide range of coating compositions (Table 1). When the current density was varied, time of current supply was adjusted to obtain a constant coating thickness of 3 to 3.5 μm. The current was not supplied continuously during plating but was switched on and off to simulate industrial conditions where the steel plate passes different electroplating cells.

2.2 Characterization of the Zinc-Cobalt Alloy Deposits

The cobalt content was varied between 0.2 and 7 wt% by changing the plating conditions. The coating weight was determined as the weight difference of the samples before and after

Table 1 Process parameters for electroplating

Parameter	Range
pH	2-4
Current density	53-133 A/dm^2
Electrolyte flow rate	1.5-4.3 m/s

For a coating thickness of 3.5 μm at T = 55 °C

dissolving the coating in diluted hydrochloric acid (HCl) (Ref 10). The coating composition was determined by atomic absorption spectroscopy (AAS) analysis of the solution.

Using the effective current density registered during electroplating, the authors calculated cathode current efficiency (cce), according to Faraday's law, as the following:

$$cce = \frac{m \cdot (\text{wt\%Co}/58.93 + \text{wt\%Zn}/65.38) \cdot 2 \cdot 96{,}500}{i_{\text{eff}} \cdot t} \quad \text{(Eq 1)}$$

where m is coating weight in g/dm^2; i_{eff} is effective current density in A/dm^2; and t is time during which current was applied, in seconds.

The surface morphology of the as-plated deposits was examined by scanning electronic microscopy (SEM) on a Zeiss DSM 962 SEM (Carl Zeiss Inc., Thornwood, NY). Electron backscattered images were made to study the material in cross section.

The crystallographic texture was determined by x-ray diffraction using a powder diffractometer Siemens D5000 (Brüker Spectrospin, Brussels, Belgium) equipped with a copper tube. 2-theta scans were obtained between 30 and 130°. The texture coefficient (TC_*hkl*) of the most important orientations was calculated by comparing the measured diffraction spectrum of the sample with the ASTM/Joint Committee on Powder Diffraction Standards (ASTM/JCPDS) chart of pure zinc powder (Ref 11, 12). For each orientation, the measured intensities were divided by the intensities of pure zinc powder. A random texture is characterized by $TC = 1$.

Finally, three-dimensional roughness measurements were done using a WYKO RST+ RS105138 (WYKO Corp., Tucson, AZ) in order to discern a possible influence of layer composition on the surface roughness. Three-dimensional measurements do not imply filtering of the profile, so no cutoff wavelength was used. Values for surface roughness, R_a, and ten-point height, R_z, (three-dimensional) were used to characterize the roughness. A reference line was defined as the line that cut the profile in equal surfaces above and below this line. The R_a value was calculated over a well-defined length, the evaluation length, as the arithmetic mean of the departures of the profile from the reference line. Finally the R_z value was calculated by dividing the evaluation length in five equidistant parts and averaging the maximum peak to valley heights of each part.

2.3 Application Test Methods

The friction coefficient of the as-deposited coatings was measured by means of an Schwingung Reibung Verschleiβ tribometer (Optimal Instruments AG, München, Germany). The sample was submitted to a horizontal oscillating movement while making contact with a flat die subjected to an increasing vertical load. The friction coefficient f is T/N (T is the horizontal friction force, N is the applied vertical load) was measured continuously in function of the load, which increased linearly from 0.5 to 2 MPa in 15 min. The samples were lubricated with a rust preventive oil (Quaker N6130, Penzoil-Quaker State Co., Houston, TX). The die material was a cast iron GG25 of which the contact surface had a controlled roughness with an R_a value between 0.3 and 0.4 μm (at $\lambda_c = 0.8$ mm). The amount of galling was verified by three-dimensional measurements on the used tools. The friction instability coefficient (*FIC*) (Ref 13) was calculated with the following formula to evaluate the stability of the friction coefficient:

$$FIC = \int_{n=20}^{504} \left(\frac{1}{6} \sum_{i=1}^{6} \left(\frac{\partial f}{\partial n} \right)^2 \right) dn \quad \text{(Eq 2)}$$

where n is the number of measurement points (maximum 504), i is the number of tests (maximum 6), and f is the friction coef-

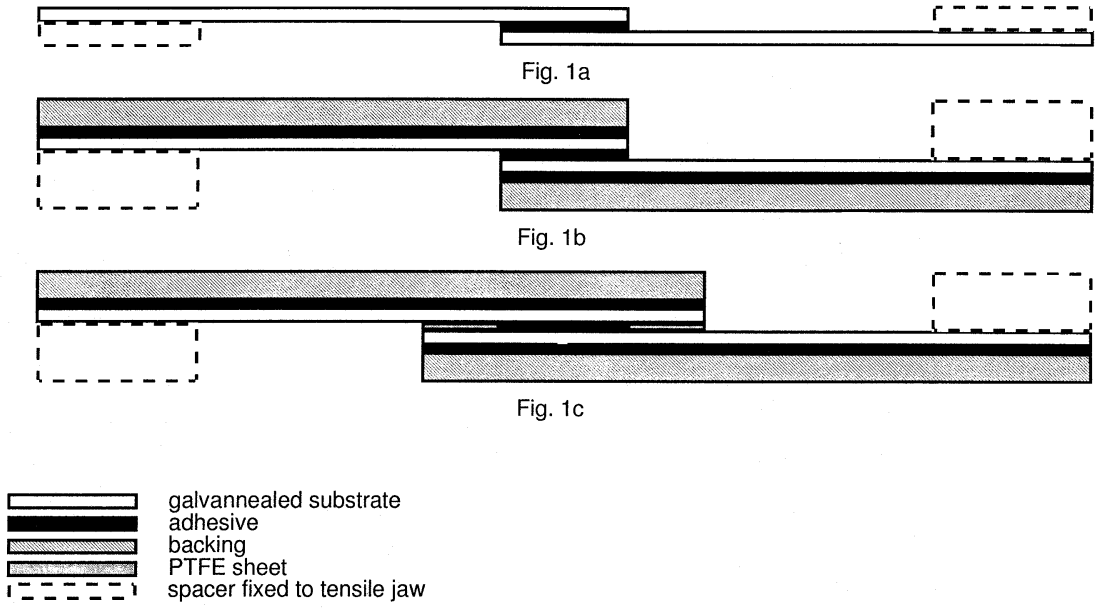

Fig. 1 Lap shear test sample geometries. (a) Spacers. (b) Backing strips. (c) Polytetrafluoroethylene sheet

ficient. High values of *FIC* suggest the formation of cold welds during the test, and, thus, FIC gives an indication of the sensitivity of the material to galling.

The powdering behavior was evaluated by a 60° V-bend test. This test has the advantage of evaluating the resistance against delamination in bending and unbending in the absence of frictional effects (Ref 14). The sensitivity to powdering was characterized as the weight loss of the specimen after applying and removing an adhesive tape (Permacel 99, 26 mm wide Permacel, A Nitto Denko Co., New Brunswick, NJ) at the fold on the V-bend sample.

The sensitivity for cracking was characterized by SEM. The number of cracks, crack length, and the width of the cracks on the bend of 60° V-bend samples were evaluated.

Adhesion of the coating was tested by means of a lap shear test. A number of corrections were applied to the sample geometry to avoid the major disadvantages of the single lap joint, as described in ASTM D 1002 (Ref 15). This is shown in Fig. 1 (Ref 16). Spacers (Fig. 1a) were applied to the jaws of the tensile testing machine to correct for the asymmetric design. Backing strips (Fig. 1b) were used to increase the stiffness of the samples and thus decreased the influence of the substrate thickness. Finally polytetrafluoroethylene (PTFE) sheet (Fig. 1c) was used, located next to the adhesive, to obtain an adhesive layer with flat straight edges and a precisely controlled thickness and overlap length. Tests were carried out on samples with an overlap length of 25 mm and an adhesive thickness of 0.2 mm, Terokal 4520-34 (Henkel Teroson, GmbH, Heidelberg, Germany) being used as adhesive.

The corrosion resistance of the unpainted samples was evaluated by electrochemical measurement using an EG & G 273 A potentiostat (EG & G Instruments, Oak Ridge, TN). The corrosion rate was determined by means of polarization resistance measurement. The Stearn-Geary equation (Eq 3) was used to calculate i_{corr} and the corrosion rate as follows:

$$\frac{\Delta E}{\Delta I} = \frac{\beta_a \cdot \beta_c}{2.3 \cdot i_{corr} \cdot (\beta_a + \beta_c)} \qquad \text{(Eq 3)}$$

where $\Delta E/\Delta I$ = the measured polarization resistance ($M\Omega$); β_a = anodic Tafel constant (V/decade); β_c = cathodic Tafel constant (V/decade); and i_{corr} = corrosion current (μA).

A number of samples were dip phosphated using a conventional trication (Zn, Mn, Ni) process on a laboratory coating line. The phosphate solution consisted of Primaire M, Granodine 1994 A, Granodine starter 655, Granodine 1994 E2, toner 95HA (Henkel Metal Chemicals, Brussels, Belgium), and demi-water. The phosphate morphology was studied by SEM.

3. Results and Discussion

3.1 Influence of Plating Conditions

Cobalt content of the electrodeposited layers reported on in the present study was between 0.2 and 7 wt%. All deposits had a cobalt content less than the $Co^{2+}/(Co^{2+} + Zn^{2+})$ ratio in the bath, thus confirming anomalous codeposition, which can be explained by the hydroxide suppression mechanism. This mechanism is based on the supposition that the cobalt deposition is retarded by the formation of a zinc-hydroxide film on the cathode surface due to an increase of pH adjacent to the cathode (Ref 17, 18).

Figure 2 illustrates the influence of current density and bath composition on the coating composition. For both bath compositions, the cobalt content in the coating shows a linear increase with increasing current density. This suggests that the current density exceeds the limiting current for Zn^{2+} reduction from the zinc-hydroxide film, and Co^{2+} reduction becomes more important with increasing current density. When the zinc-cobalt ratio is increased by lowering the cobalt content in the bath, smaller cobalt contents were achieved (Fig. 2). Dilution of the electrolyte, however, resulting in an electrolyte with a lower wt% of zinc and cobalt but similar zinc/cobalt ratios, showed no influence on the cobalt content in the coating. The explanation of these phenomena is based on the hydroxide suppression mechanism, which is schematically represented in Fig. 3. Two features of the mechanism have to be emphasized. First, according to Fukushima et al. (Ref 19), the coatings deposited in region II have a lower cobalt content when the wt% cobalt in the bath is decreased. This results in a shift of the curve to lower values (1 → 2), explaining the experimentally observed de-

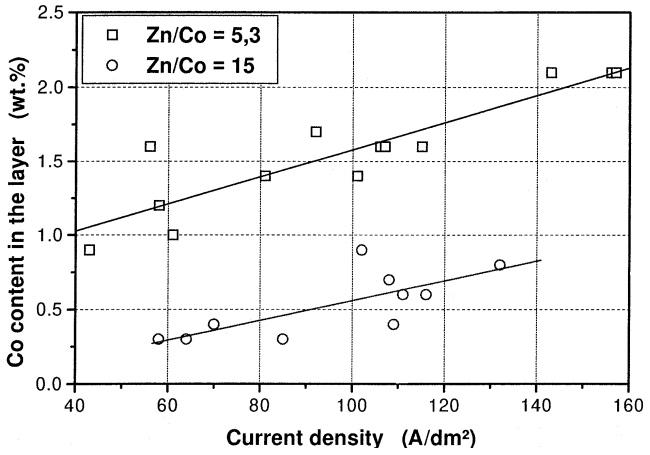

Fig. 2 Influence of current density and zinc to cobalt ratio on the cobalt content in the coating

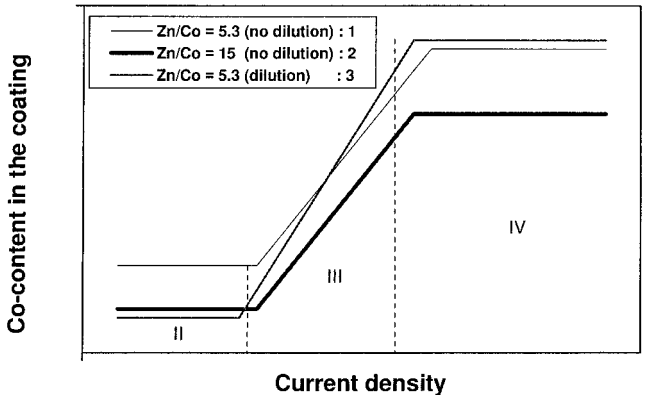

Fig. 3 Schematic representation of the effect of zinc to cobalt ratio and dilution on the anomalous codeposition mechanism

crease in cobalt content in the coating when the zinc-cobalt ratio is increased. Second, a decrease of the wt% zinc in the bath causes a shift of the limiting current density for Zn^{2+} reduction to lower values, and, thus, region III will be reached at lower current densities. When dilution of the electrolyte takes place, both wt% cobalt in the bath and wt% zinc in the bath are decreased, a situation that results in curve 3. As can be noticed in Fig. 3, curves 1 and 3 approach each other in region III, resulting in the same cobalt contents of the deposits whether the electrolyte is diluted or not.

Figure 4 shows the influence of change in pH and the influence of change in flow rate of the electrolyte. When the flow rate is increased, the limiting current for the Zn^{2+} reduction is shifted to higher values, and the supply of H^+ is increased resulting in a retarded depletion of H^+ and a thicker zinc hydroxide film at the same current density and a lower cobalt content in the deposit.

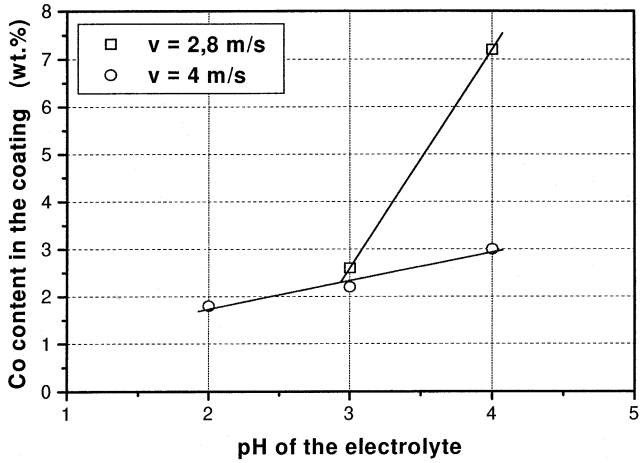

Fig. 4 Influence of pH and electrolyte flow rate on the cobalt content in the coating

Figure 5 shows the cobalt distribution in a layer deposited from a bath with pH = 2 (Fig. 5a) and a layer deposited from a bath with pH = 3 (Fig. 5b). In the case of pH = 3 at the interface with the steel, a cobalt-rich layer is found (Fig. 5b). As the increase of the pH of the electrolyte causes the driving force for H_2 evolution to fall significantly, the initial electrodeposition process is dominated by the preferential cobalt deposition. However, once an increase in pH induces the formation of a zinc hydroxide layer, the deposition changes to anomalous deposition, and the cobalt content in the layer is restricted to the same value as in a layer deposited at a pH = 2.

Layers deposited at lower pH (pH = 2), however, show a homogeneous cobalt content over the cross section of the coating (Fig. 5a).

Cathode Current Efficiency. No influence of plating variables on the cathode current efficiency was found. In all cases, cathode current efficiencies were between 88 and 95%, thus lower than for the electroplating of zinc (approximately 98%) but higher than for the electroplating of zinc-nickel (approximately 83%).

3.2 Characterization of the Zinc-Cobalt Alloy Layers

Visual Appearance. All deposits showed a light gray appearance, somewhat darker than that of pure zinc deposits. At high pH values combined with low flow rates (less than 2 m/s), layers were found that had a dark and powdery surface appearance that could easily be rubbed off.

Phase Composition and Morphology of the Electrodeposited Layers. In order to evaluate the influence of the cobalt content on the morphology of the coating, the latter was examined on coatings deposited with different plating variables, which resulted in zinc-cobalt alloy layers with different cobalt contents. As shown in Fig. 6, the surface morphology of such layers is very similar to the terraced surface morphology of electrodeposited pure zinc. With increasing cobalt content, however, the zinc-cobalt alloy crystals become smaller, and the surface becomes more nodular. Study with the SEM also revealed the presence of large circular, through-thickness pores

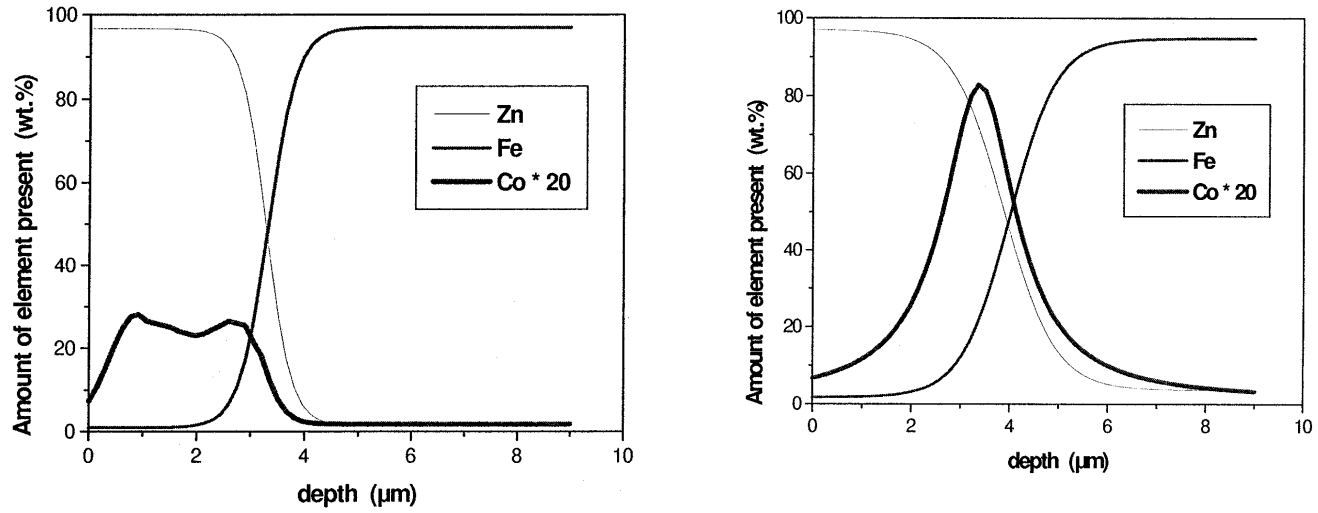

Fig. 5 Cobalt depth distribution, measured with GDOES. Coating deposited at (a) pH = 2 and (b) pH = 3

with a diameter up to 200 μm (Fig. 6). At the border of some defects, cobalt enrichments were found, while in the circular area of the defect, no zinc or cobalt was deposited. The circular geometry of the defects suggests that they might be caused by the formation of hydrogen bubbles at the cathode surface. At the start of the deposition process both Co^{2+} reduction and H_2 formation dominate the plating process. This is supported by the fact that both glow-discharge emission spectroscopy and electron probe microanalysis revealed the existence of a cobalt rich layer at the coating/substrate interface when deposited at high pH (Fig. 5). These areas of high cobalt content should favor the nucleation of the hydrogen bubbles. As the hydrogen overvoltage on cobalt is significantly lower than on zinc, cobalt rich areas can be expected to favor the nucleation of hydrogen bubbles, (Table 2). Moreover, since zinc nucleates easier on zinc than on iron or cobalt, these defects, once formed, are maintained resulting in the experimentally observed holes in the coating.

X-ray diffraction analysis revealed that the cobalt-zinc alloy coatings were solid solutions of cobalt-zinc. Furthermore, an influence of the cobalt content on the crystal orientation was found. As can be seen clearly from Fig. 7, at cobalt contents below 1 wt% the presence of cobalt in the hexagonal η phase seems to favor low index pyramidal and prismatic orientations. With increasing cobalt content, the low index pyramidal orientation dominates, while the prismatic orientation disappears. Basal crystal orientations were observed only at low cobalt contents.

Roughness of the As-Deposited Layers. Three-dimensional roughness measurements were carried out on a number of samples with various cobalt content. The results are shown in Fig. 8. The R_a value and the R_z value vary respectively from 1.69 to 1.83 and from 15.34 to 18.9 μm. For both roughness parameters, all measured values were higher for the samples with cobalt content than they were for samples of pure zinc, and a significant, positive correlation between cobalt content and roughness was found to confirm the more nodular morphology at higher cobalt contents.

Table 2 Hydrogen overvoltages for cobalt, iron, and zinc at a current density = 50 A/dm^2

Element	Hydrogen overvoltage, V
Cobalt	0.48
Iron	0.5
Zinc	1.24

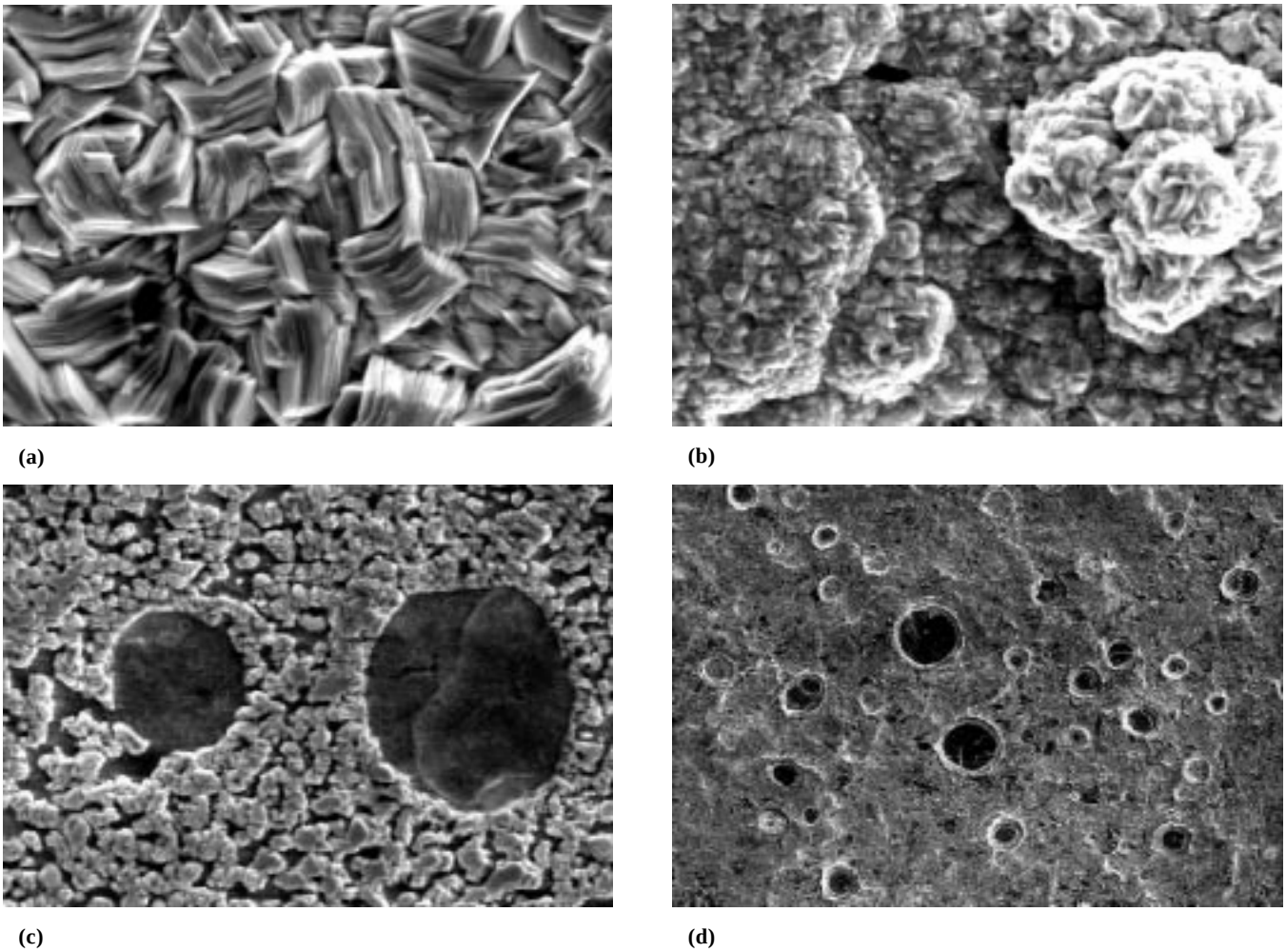

Fig. 6 Morphology of zinc-cobalt alloy coatings. SEM micrographs with SE contrast. (a) Pure zinc coating (5000×). (b) Zinc-cobalt alloy coating, 3.6 wt% Co (5000×). (c) SEM of circular holes in a zinc-cobalt coating (2000×). (d) SEM of circular holes in a zinc-cobalt coating (2000×)

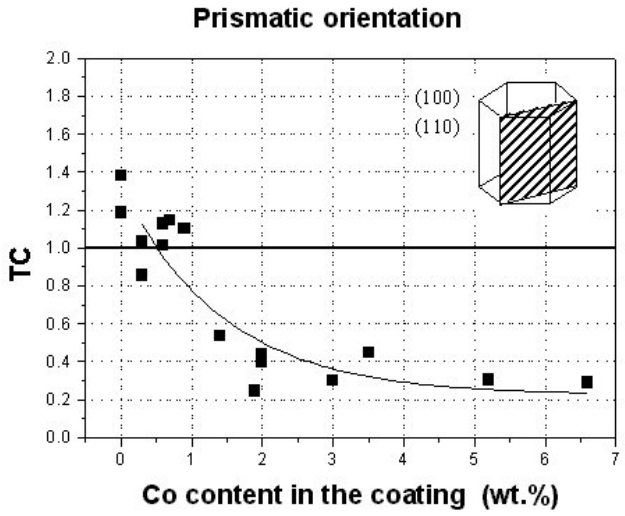

(a)

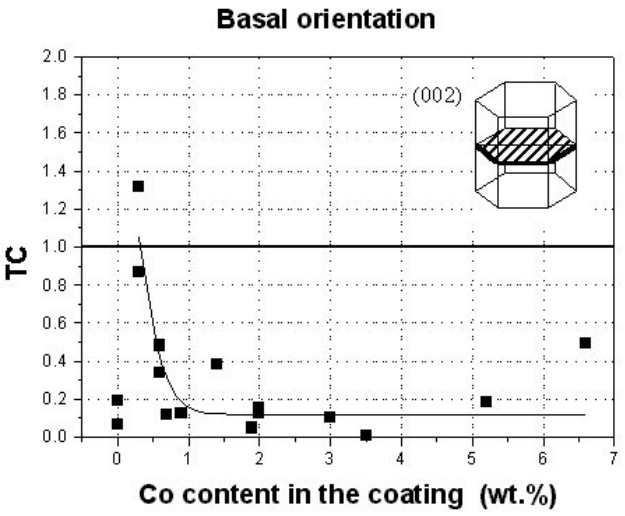

(b)

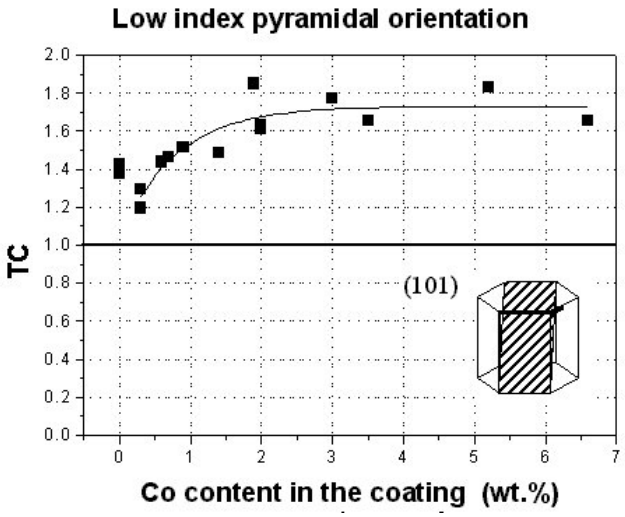

(c)

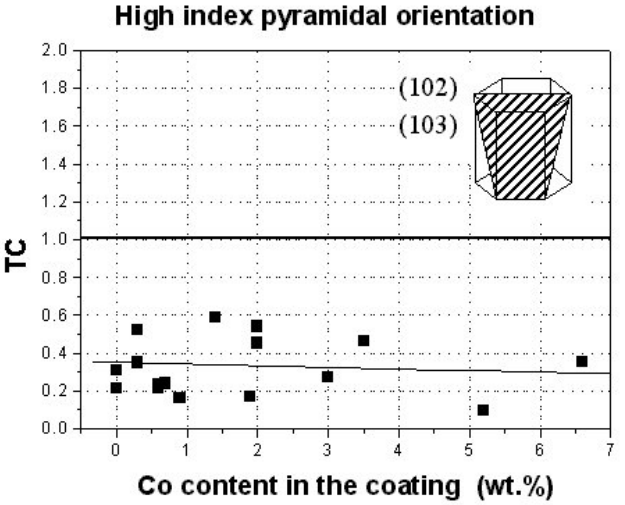

(d)

Fig. 7 Influence of cobalt content on the texture of the layer

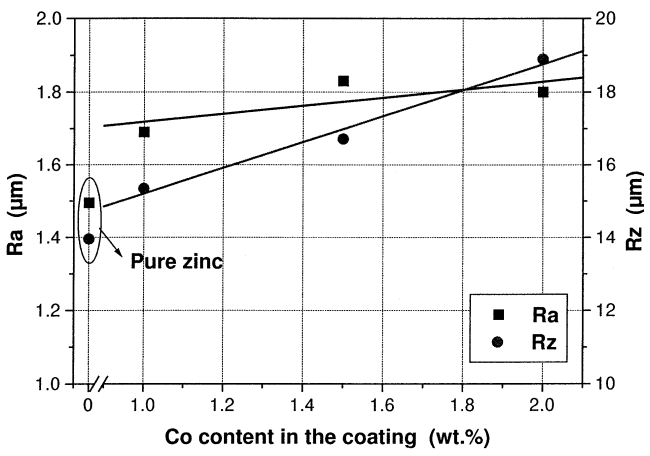

Fig. 8 Influence of cobalt content on the roughness of the coating

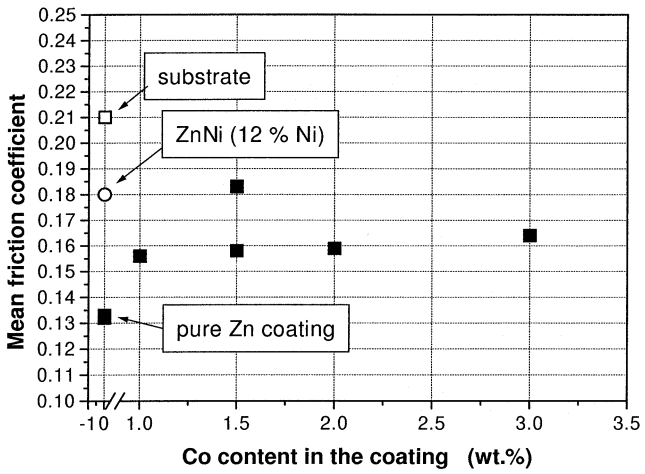

Fig. 9 Influence of cobalt content on the friction coefficient

3.3 Application Behavior

The formability of the coated sheet steel is a very important issue for automotive applications. The importance of friction in many sheet forming processes is well documented, and high values of friction coefficient result in material loss and excessive wear. Galling occurs when cold welds are formed, and the particles caused by rupture of the welds remain on the die. Especially soft and ductile materials are sensitive to galling (Ref 20); hard materials, however, tend to be subject to powdering (Ref 21). This makes necessary the evaluation of the friction coefficient and the galling, powdering, and flaking behavior of the coated material during forming operations.

Friction Coefficient and Galling. As can be seen in Fig. 9, no significant influence of the cobalt content on the friction coefficient was found. Compared to pure zinc coatings, however, zinc-cobalt alloy coatings have higher friction coefficients. Compared to zinc-nickel or the steel substrate, the friction coefficient is lower. At higher cobalt content, the calculated FIC values ($\pm 5 \times 10^{-3}$) revealed a more unstable friction than was the case for pure zinc coatings ($\pm 10^{-3}$), but a far lower friction level than that for the steel substrate ($>10^{-2}$). Thus, no sensitivity to galling could be deduced from the FIC values.

Powdering behavior was evaluated by means of a 60° V-bend test on samples containing between 0.4 and 2.7 wt% cobalt in the coating. Figure 10 shows the relation between the amount of cobalt and the weight loss of the coating. A degreasing of the steel for 10 s before electroplating resulted in higher values of weight loss than in the case of degreasing during a fixed time of 30 s. This shows the importance of a clean, well-degreased surface that is free from oil. For the latter, values were obtained as low as 0.3 mg/50 mm, thus similar to pure zinc coatings, at low cobalt contents, but values as high as 2.5 mg/50 mm, similar to galvannealed layers, were found at higher cobalt contents.

Cracking. Some of the folded samples were characterized with SEM (Fig. 11) in order to evaluate the sensitivity to cracking. It seemed that rising cobalt content caused the coating to become more sensitive to cracking. This was determined by comparing the SEM pictures of samples with different cobalt content on the basis of crack length, crack width, and number of cracks intersecting a straight line that was drawn on the pictures. No difference was found between a pure zinc coating 50/50 high pyramidal angle and prismatic orientation) and a zinc-cobalt alloy coating with 0.4 wt% Co, except for a slight decrease in number of cracks for the latter. Compared with a Zn-Co alloy coating with 0.8 wt% Co in the layer, this coating showed significantly more cracks than the first two. Simultaneously, the width of the cracks was found to be higher for the 0.8 wt% Co coating, rising up to 20 μm instead of 10 μm in the case of 0.4 wt% cobalt. It is not yet clear if there is a connection between the texture of the coating and the crack sensitivity. Further investigation will be necessary to determine whether a relation exists.

Adhesion of the Coating. A lap shear test was performed on zinc-cobalt alloy coatings with different Co content to evaluate the influence of the Co content on the adhesion. As

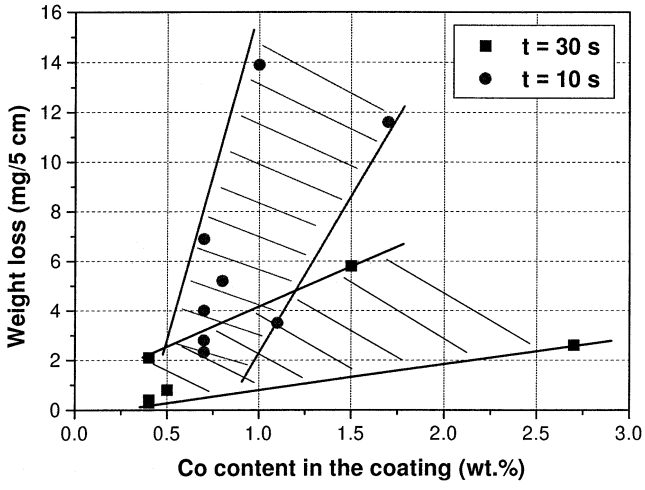

Fig. 10 Influence of cobalt content on the adhesion properties of the coating, evaluated by a V-bend test

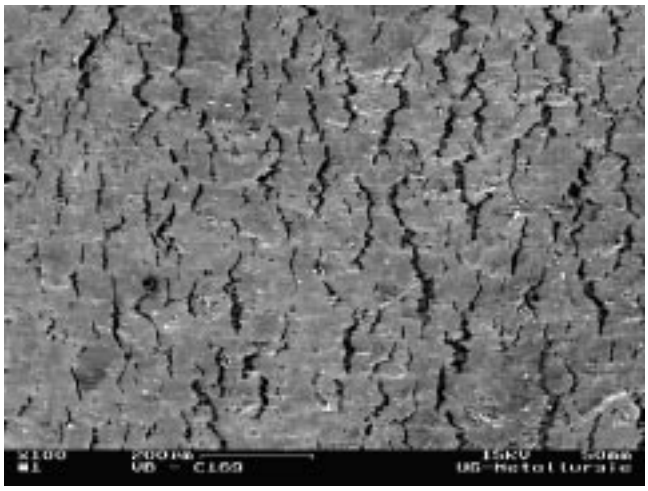

(a)

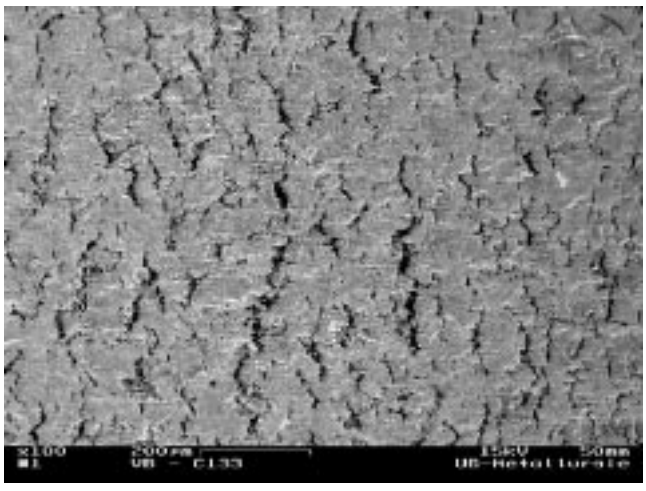

(b)

Fig. 11 Difference in cracking sensitivity between zinc-cobalt alloy coatings with different cobalt content. SEM micrographs of sheet samples after a 60° bending.

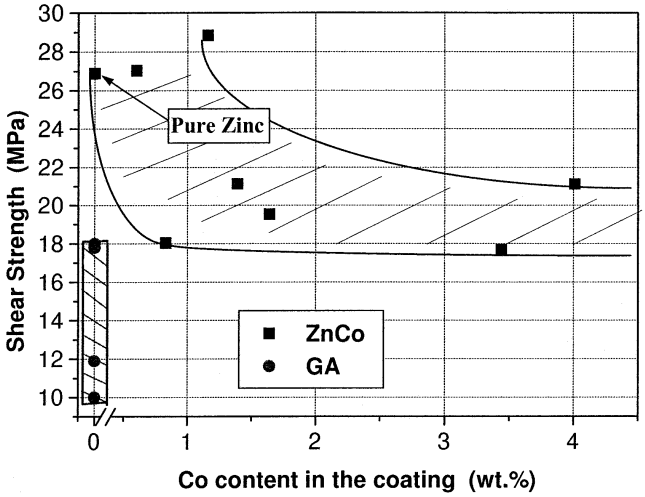

Fig. 12 Influence of cobalt content on the adhesion of the coating as evaluated by a lap shear test. The shear strength values for galvannealed coatings (GA) are substrate dependent.

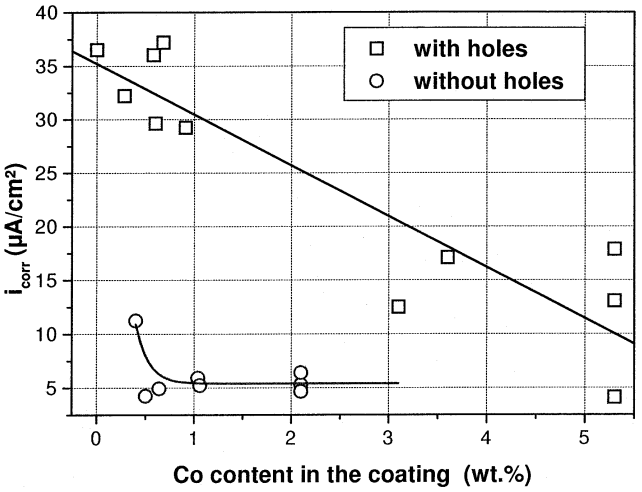

Fig. 13 Influence of cobalt content in the coating on i_{corr}, the corrosion current density

shown in Fig. 12, no correlation was revealed between the Co content in the coating and the shear strength. Most measured values lay in the range of 20 MPa. This is comparable to values obtained for the adhesion of zinc-nickel coatings but less than the shear strength measured for a pure Zn coating. However, compared to the measured values for galvannealed coatings on different types of steel substrate, the measured values of shear strength were significantly higher. The fracture planes of all samples showed a mixture of adhesive and cohesive failure, meaning that fracture took place partly in the adhesive and partly at the coating/substrate interface.

Electrochemical Measurements and Corrosion Rate. The influence of the Co content on the corrosion resistance of the as-deposited coating is shown in Fig. 13. Two groups of measurements can clearly be distinguished in Fig. 13. The first group are measurements on samples with holes in the coating resulting in corrosion current densities between 37 and 17 µA/cm^2. This corresponds to corrosion rates of 1.1 and 0.5 mm/year, respectively. A significant decrease in corrosion rate was observed with increasing Co content. The second group of samples (with no holes in the coating) showed a far smaller corrosion current density and a corrosion rate of ±0.15 mm/year. In this case the corrosion resistance of the samples exceeded that of pure Zn, with a corrosion rate which was smaller by a factor of 5 to 7.

When the corrosion current densities are plotted as a function of the coating texture values for the different orientations (Fig. 14), it can be seen that the prismatic and the low index pyramidal orientations have a clear effect on the corrosion rate. Low index pyramidal orientations seem to favor low corrosion rates, whereas prismatic orientations increase the corrosion rate.

The other two orientations have a far less distinct influence. It is, however, not clear whether the change in texture caused change in corrosion rate or whether change in corrosion rate resulted from the higher cobalt content in the coating, because changes in texture were connected to the change in cobalt content of the alloy coating.

Phosphatability. Zn-Co alloy coatings with 0.5 to 1.7 wt% cobalt were dip phosphated in a pilot line. In all cases needle-shaped phosphate crystals were formed. The reactivity of the phosphate solution for the steel substrate was approximately the same as on a pure zinc coating, but the size of the needles of the phosphate layer was significantly smaller, as can be seen from Fig. 15.

4. Conclusions

The influence of cobalt content on the application properties of electrodeposited zinc-cobalt alloy layers has been studied in detail, and the main conclusions are the following:

- The cobalt content can be varied between 0.2 and 7 wt% by changing the process parameters during electrodeposition. Current density and pH of the electrolyte have a positive influence electrolyte flow rate, and zinc-cobalt ratio have a negative influence on the cobalt content. High values of pH tend to favor normal codeposition, resulting in an inhomogeneous distribution of cobalt over the thickness of the coating. Cobalt-rich layers are formed near the substrate, while near the surface, the cobalt content corresponds to that obtained at low pHs.
- The application tests showed that zinc-cobalt alloy coatings have a higher roughness and friction coefficient but a lower adhesion level when compared to pure zinc coatings. On the other hand, the corrosion resistance of a homogeneous film-forming zinc-cobalt alloy coating is significantly better than that of a pure zinc coating.
- Finally, the results of this study show that at low pH and at a sufficiently high current density, zinc-cobalt alloy coatings with ±2 wt% cobalt can easily be plated on sheet steel substrates. These layers are characterized by a favorable combination of application properties, which are very similar to those to those of pure zinc coatings, and a far better corrosion resistance. Thus, zinc-cobalt alloy coatings offer the possibility of a substantial coating thickness reduction.

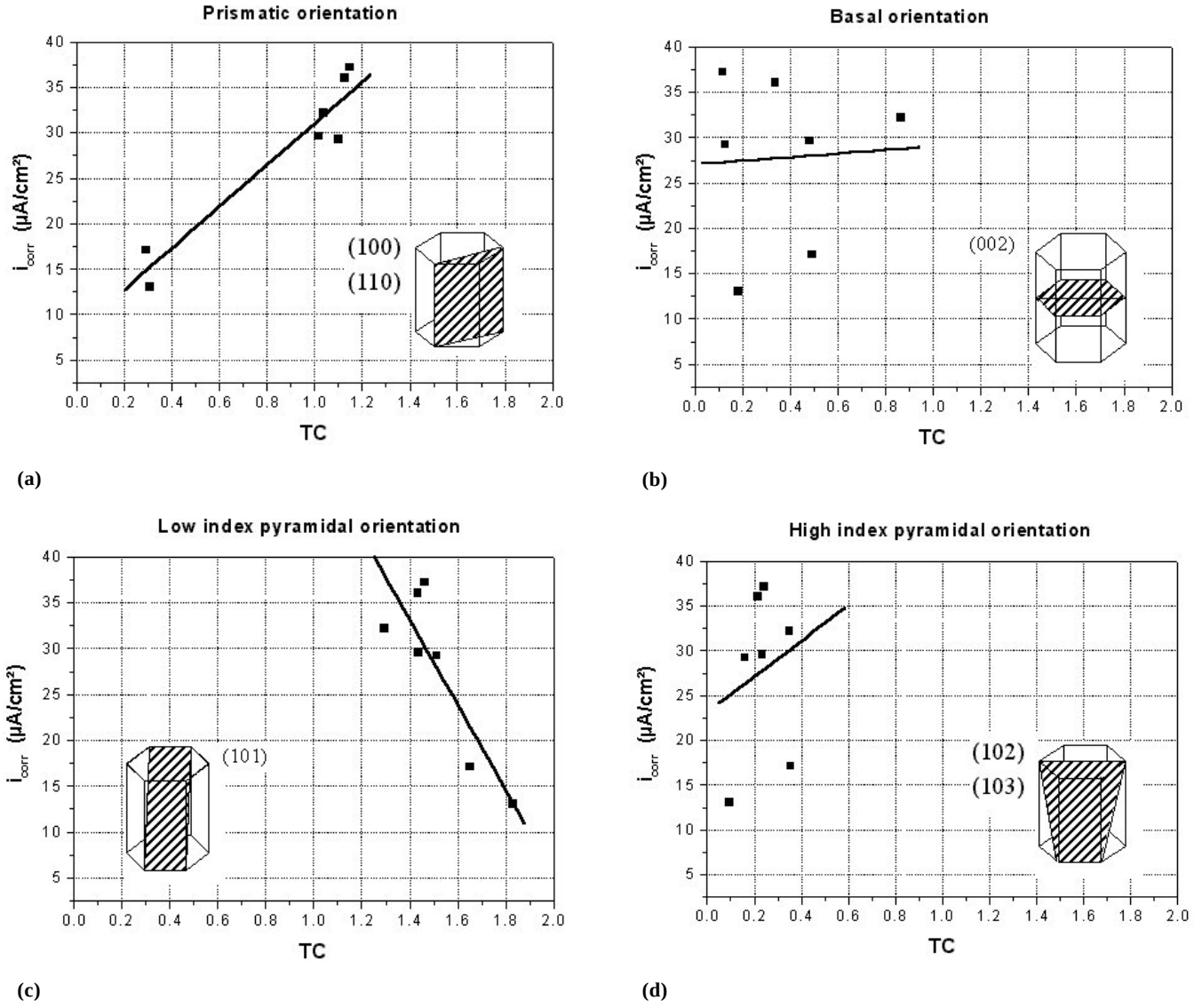

Fig. 14 Influence of texture of the coating on i_{corr}, the corrosion current density

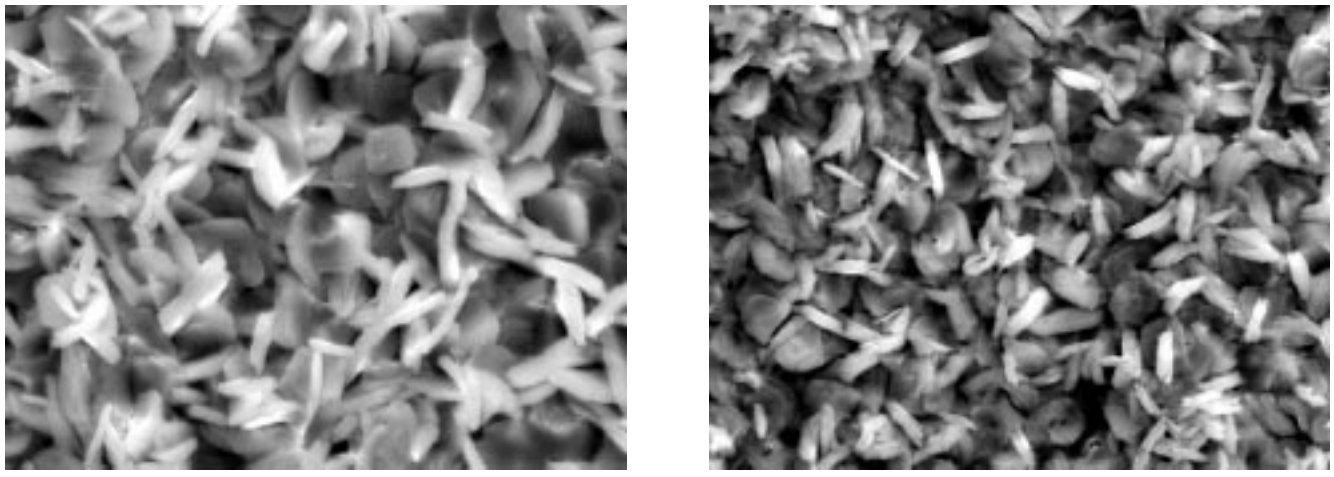

Fig. 15 SEM micrographs (SE contrast) of phosphated zinc and zinc-cobalt alloy coatings. (a) Phosphate layer on a zinc coating (5000×). (b) Phosphate layer on a zinc-cobalt alloy coating (5000×)

Acknowledgments

The authors thank C. Xhoffer, K. De Blauwe, J. Scheers, and L. Berckmoes (OCAS) for the valuable contributions. The authors also gratefully acknowledge E. Herrebout, J. Craenen, A. De Groote, and C. Sonck (University of Ghent) for their valuable assistance in this investigation.

References

1. J.H. Lindsay, Coated Steel Sheet in the Automotive Industry, *The Use and Manufacture of Zinc and Zinc Alloy Coated Sheet Steel Products into the 21st Century (Galvatech '95)*, (Chicago, IL, September 1995, p 579-588
2. T. Asamura, New Zinc-Coated Steels and Their Processing Technologies in Japan, Proceedings of the Fourth *International Conf. on Zinc and Zinc Alloy Coated Steel Sheet (Galvatech '98)*, (Tokyo), Sept 1998, p 14-21
3. D. Crotty and R. Griffin, Performance Characteristics of Zinc Alloys, *Plat. Surf. Finish.*, April 1997, p 57-61
4. B.C. De Cooman, "Coated Sheet Steel: An Overview of the Current Products and their Performance," Prof. Dr. Ir. J. Dilewijns: Liber Amicorum, 1997, p 287-310
5. S.A. Watson, "Zinc-Nickel Alloy Electroplated Steel Coil and Other Precoated Coil for Use by the Automotive Industry: A Review of Literature Published 1983 to 1987," Nickel Development Institute, European Technical Information Center, Alvechurch, Birmingham, England, March 1988
6. T.J. Natorski, Zinc and Zinc Alloy Plating in the 90s, *Met. Finish.*, March 1992, p 15-17
7. J. Giridhar and W.J. Van Ooij, "A New NiZn/ZnCo Coated Steel Wire for Tire Cord Applications," *Wire J. Int.*, Vol 26 (No. 6), 1993, p 30-37
8. J. Giridhar, W.J. Van Ooij, and M. Cipparone, "Adhesion Behaviour of a New Corrosion-Resistant Steel Tire Cord Coated with NiZn/ZnCo Alloy Layers," Rubbercon '93, International Rubber Conference (New Delhi, India), 1993
9. J. Giridhar and W.J. Van Ooij, Study of Zn-Ni and Zn-Co Alloy Coatings Electrodeposited on Steel Strips, Part I: Alloy Electrodeposition and Adhesion of Coatings to Natural Rubber Compounds, *Surf. Coat. Technol.*, Vol 52, 1992, p 17-30
10. A. DeBoeck, L. Vanlerberghe, and M. Vanthournout, Quantitative Analysis of Zinc and Zinc Alloy Coatings on Steel, *La Revue de Métallurgie—CIT*, Oct 1993, p 1277-1282
11. A. DeBoeck, M. Vanthournout, and J.M. Van der Hoeven, "The Influence of Texture on the Deformation Behaviour of Electrodeposited Zinc Coatings," *IDDRG Conf. Proc., (*Lisbon), May 1994, p 55
12. Ph. Bérubé and G. L'Espérance, "A Quantitative Method of Determining the Degree of Texture of Zinc Electrodeposits," *J. Electrochem. Soc.*, 1989, Vol 136, p 2314
13. C. Ortlieb and A. De Boeck, "SIKEL NV—Product and Application," 1995
14. Warnecke and W. Müschenborn, Formability Aspects of Galvannealed Steel Sheet, *IDDRG Conf. Proc.*, (Amsterdam), May 1985
15. Standard Test Method for Strength Properties of Adhesive in Shear by Tension Loading (Metal to Metal), D 1002-72, ASTM, 1983
16. K. Meseure, C. Xhoffer, B.C. De Cooman, I. Hertveldt, and J. Dilewijns, The Shear Strength of Galvannealed Coatings on IF Steels, *Proc. of Intergalva '97*
17. T. Akayima, H., Fukushima, K. Higashi, M. Karimkhani, and R. Kammel, Electrodeposition Behavior of Zinc-Iron-Group Metal Binary Alloys from Sulfate Baths, *International Conf. on Zinc and Zinc Alloy Coated Sheet Steel (Galvatech '89)* (Tokyo), Sept 1989, p 45-50
18. H. Fukushima, T. Akiyama, M. Yano, T. Ishikawa, and R. Kammel, Electrodeposition Behaviour of Zn-Iron-Group Metal Alloys from Sulfate and Chloride Baths, ISIJ International, Vol 33 (No. 9), 1993, p 1009-1015
19. H. Fukushima, T. Akiyama, K. Higashi, R. Kammel, and M. Karimkhani, Electrodeposition Behaviour of Binary Zinc Alloys with Iron-Group Metals from Sulfate Baths, *Metall. und Technik*,Vol 44 (No. 8), 1990, p 754-759
20. K. De Wit, "Electroplating and Application Properties of Zn-Fe Coatings on Steel," Ph. D. dissertation, University of Ghent, 1998, p 208 (in Dutch)
21. M. Arimura, M. Urai, J. Iwaya, and M. Iwai, "Effects of Press-Forming Factors and Flash Plating on Coating Exfoliation of Galvannealed Steel Sheets," *The Use and Manufacture of Zinc and Zinc Alloy Coated Sheet Steel Products into the 21st Century (Galvatech '95)*, (Chicago), Sept 1995, p 733